New Journal of Physics
The open-access journal for physics

Being on time in magnetic reconnection

M Faganello[1], **F Califano and F Pegoraro**
Physics Department, University of Pisa, Pisa, Italy
E-mail: matteo.faganello@df.unip.it

New Journal of Physics **11** (2009) 063008 (25pp)
Received 23 February 2009
Published 8 June 2009
Online at http://www.njp.org/
doi:10.1088/1367-2630/11/6/063008

Abstract. The role of magnetic reconnection on the evolution of the Kelvin–Helmholtz instability is investigated in a plasma configuration with a velocity shear field. It is shown that the rate at which the large-scale dynamics drives the formation of steep current sheets, leading to the onset of secondary magnetic reconnection instabilities, and the rate at which magnetic reconnection occurs compete in shaping the final state of the plasma configuration. These conclusions are reached within a two-fluid plasma description on the basis of a series of two-dimensional numerical simulations. Special attention is given to the role of the Hall term. In these simulations, the boundary conditions, the symmetry of the initial configuration and the simulation box size have been optimized in order not to affect the evolution of the system artificially.

Contents

[1] Author to whom any correspondence should be addressed.

1. Introduction

Magnetic field line reconnection is a fundamental physical process in a magnetized plasma and is able to reorganize the large-scale topology of the magnetic field and to affect the global plasma energy balance of the system at the same time. Magnetic reconnection is driven by large-scale plasma current inhomogeneities and plasma motions but requires that small-scale effects, as compared to the large-scale magnetohydrodynamics (MHDs), allow for a local decoupling between the plasma and the magnetic field evolution. Depending on the plasma regime under consideration these 'micro-physics' effects may include a non-vanishing plasma resistivity, kinetic resonances or, as is the case for the two-fluid model description adopted in this paper, electron inertia terms in the generalized Ohm's law. The role of these micro-physics processes, together with the large-scale MHD driving mechanisms, in determining the rate of magnetic reconnection is of paramount importance. In this perspective, the occurrence of 'fast' magnetic field line reconnection in low collisionality or collisionless plasmas is of special importance as it is thought to develop on timescales that do not exceed, by large factors, the dynamical timescales of the plasma configuration as determined within the ideal MHD description.

Fast magnetic reconnection [1]–[6] is expected to occur when the large-scale plasma dynamics leads to the formation of extremely narrow current sheets. When their width becomes comparable to the ion skin depth $d_i \equiv c/\omega_{pi}$, with ω_{pi} the ion plasma frequency, ions and electrons need no longer have almost equal fluid velocities, as is the case in the MHD plasma description. In particular, on such spatial scales ions can decouple their motion from the evolution of the magnetic field, while electrons remain tied to the magnetic field until spatial scales as small as the electron skin depth d_e are reached. Here, as mentioned above, we have assumed that the relevant microphysics effect in the generalized Ohm's law that breaks the coupling between the electron and the magnetic field evolution is given by electron inertia so that magnetic reconnection takes place only when the d_e-scale ($d_e \equiv c/\omega_{pe}$) is reached. In plasma configurations with not too small values of the β parameter, defined as the ratio between the plasma and the magnetic pressure, the wider ion decoupling region allows the ion inflow velocity at the reconnection point to be comparable with the local Alfvén velocity, and thus allows magnetic reconnection to occur on faster timescales [1]–[7] than predicted by a single fluid description.

Magnetic reconnection is usually studied either as an initial value problem, in which case a specific large-scale magnetic configuration (an ideal MHD equilibrium) with large current gradients is considered such that a magnetic reconnection instability develops spontaneously, or as a forced problem where a specific velocity field is imposed from the boundary on a magnetic configuration with a sheared magnetic field. These approaches separate somewhat artificially the reconnection process from the global evolution of the system as a whole. On the contrary, here we are interested in studying the feedback between large- and small-scale dynamics self-consistently. With this aim, we look for large-scale structures that are not prescribed *a priori* and that develop on a timescale comparable with the small-scale magnetic field evolution. In this case magnetic reconnection occurs naturally as a consequence of the large-scale evolution of the system and at the same time can affect the system back and can determine its long-term evolution [8].

The large-scale evolution of interest can be provided by the development of an ideal MHD instability. An important example is given by the nonlinear evolution of Kelvin–Helmholtz (K–H) vortices that form along the flank of the Earth's magnetosphere at low latitude [9]–[12].

The study of the role of magnetic reconnection on the evolution of the K–H instability is in fact the central theme of the present paper.

The evolution of these large-scale structures is influenced by magnetic reconnection that occurs locally both inside and between these vortices. In particular, we are interested in studying the competition between the process of vortex pairing (which represents the 'natural' 2D hydrodynamic [13, 14] and MHD [15]–[17] evolution of K–H vortices) and the onset of the secondary magnetic field line reconnection instability driven by the current inhomogeneities produced by the vortex winding and pairing.

The linear evolution of a large-scale K–H instability and the early evolution of the vortices is essentially an MHD process and depends only on the initial velocity and magnetic field, regardless of the specific small-scale physics [21]–[24].

If the value of the in-plane magnetic field parallel to the initial flow is low enough, the K–H instability can grow during its linear phase [9] and develops into vortices that advect the magnetic field and thus stretch and roll up the magnetic field lines [9], [18]–[21]. This large-scale evolution is able to build up favorable conditions for reconnection to occur producing inversion layers of the in-plane magnetic field both inside and between the vortices. Thus magnetic reconnection acts as a secondary instability on the primary K–H instability. Since the plasma dynamics is essentially driven by the vortex motion, the reconnection events that are produced in these layers are usually denoted as vortex induced reconnection (VIR) [12], [21]–[23], [25]. Magnetic reconnection allows the topology of the magnetic field to change, which is a necessary condition for plasma mixing to occur and in this way affects the evolution of the vortices themselves.

The role of the magnetic field on vortex dynamics has been studied numerically mostly in the limit of one vortex only, the largest one contained in the simulation box. It has been shown that, even if the magnetic field is weak and unable to prevent the formation of a rolled up vortex, nevertheless the VIR process eventually leads to vortex disruption [22, 23, 26, 27]. Actually, in a homogeneous density configuration, three different regimes were found [18]–[21]. In the 'strong field' regime ($2 < M_{A,\parallel} < 4$, with $M_{A,\parallel}$ the in-plane Alfvénic Mach number) the system is nonlinearly stable and the K–H instability cannot develop into a rolled up vortex. In the 'weak field' or 'disruptive' regime ($4 < M_{A,\parallel} < 20$), the K–H instability develops into a rolled up vortex that is subsequently disrupted by VIR. This disruptive process is believed to be one of the causes of the formation of a mixing layer in the downstream region of the magnetotail. In the 'very weak field' or 'dissipative' regime ($M_{A,\parallel} > 20$–30), the behavior of the vortex is essentially hydrodynamic, the presence of the in-plane magnetic field and reconnection events can only enhance dissipation.

The importance of fast magnetic reconnection during the development of K–H vortices has been shown in [8, 28]. Although large-scale (as compared to the ion skin depth d_i) vortices are essentially MHD structures, their motion is not only able to create favorable conditions for reconnection to act, i.e. to generate magnetic inversion layers, but it is also able to build up sub-d_i current sheets, within which processes characteristic of two-fluid dynamics can develop. When such sub-d_i current layers are created, fast magnetic reconnection can occur [8, 28]. How fast the reconnection process develops is of crucial importance for the long-term evolution of the system: in order to change the global magnetic field topology reconnection must develop within a 'time window' set by the large-scale motion, i.e. before the large-scale motion destroys the favorable conditions that it has just created [8]. This result provides a clear cut example of the feedback between large- and small-scale physics, as the necessary conditions for reconnection to

occur are produced by the large-scale motion of the vortices, but the specific physical processes that make reconnection act faster or slower determine eventually the evolution of the entire system and the final magnetic field structure.

Rolled up vortices are not only needed for VIR to occur, but also necessary for the development of other kinds of secondary hydrodynamic instabilities which can grow along the vortex arms. In the presence of a density inhomogeneity the centrifugal acceleration produced by the vortex motion can give rise to Rayleigh–Taylor (R–T) type instabilities. These instabilities were studied in [29, 30] in a strictly perpendicular magnetic field configuration with a density inhomogeneity along the direction of the velocity shear, chosen so as to exclude phenomena such as VIR that are related to the in-plane magnetic field. How quickly secondary instabilities, such as VIR or R–T instabilities, will grow is crucial since they may destroy the structure of the vortices before they coalesce and, referring e.g. to the dynamics at the flank of the Earth's magnetosphere, may be the most important factor in the increase of the width of the mixing layer [30]. Rolled up vortices, generated by the K–H instability, are the necessary seeds for plasma transport in this region. During their nonlinear evolution three different processes can compete in the formation of a mixing layer: the vortex pairing process [15]–[17], the vortex disruption caused by VIR [12], [21]–[23], [25] and the vortex disruption caused by secondary hydrodynamic instabilities, such as for example the R–T instability [29, 30].

In the present paper, we study the competition between these processes during the evolution of five 'unequal' vortices. This configuration is less idealized than the one considered in other multiple-vortex studies [8, 28], where only two 'equal' vortices were considered. This new choice allows us to investigate the competition between the different processes during subsequent pairing events that involve unequal vortices. This more general setting makes it possible to prevent a too constrained choice of the initial configuration influencing the evolution of the system. In order to emphasize the role of VIR in the present paper we consider a homogeneous density plasma.

We show that, while in the presence of a sufficiently large density gradient [30] the secondary R–T instability would be able to destroy the structure of the single vortices and therefore suppress the pairing mechanism, the VIR instability in the 'disruptive' regime does not destroy the vortices before they coalesce. Furthermore, we show that if the in-plane equilibrium magnetic field has no inversion points, VIR acts only during the pairing process, in agreement with multiple vortex study of [21]. Indeed, instead of disrupting a single K–H vortex, reconnection occurs mainly as a consequence of the pairing process. This indicates the necessity of considering multiple vortex configurations in the investigations of the development of VIR. Finally, we show that the physical phenomena that occur at small spatial scales influence the final magnetic topology.

We remark that some features of our results are at variance with those recently presented in [31] where it is stated that VIR is able to suppress the pairing process and to disrupt the vortices. The results in [31] were obtained in the limit of a vanishing perpendicular (out of the plane) magnetic field (i.e. in the limit of vanishing guide field, in the terminology of magnetic reconnection) within a collisionless two-fluid description. Although in a fluid framework this limit is to be considered unphysical, we performed a similar simulation and did not observe any disruption, while the pairing process remained effective. This discrepancy appears to be due to the special initial conditions adopted in [31] that takes the initial amplitude of the fast growing mode (FGM, characterized by the biggest linear growth rate) much bigger than the amplitudes of the other modes.

In order to explore the whole 'disruptive' (weak field) regime, in the numerical simulations reported here we consider three different values of the Mach number $M_{A,\parallel} = 20.0$, 10.0 and 5.0. These choices allow the K–H instability to develop into rolled up vortices. In order to study the feedback between the large- and small-scale dynamics, we exploit the fact that the onset of the K–H instability and the subsequent evolution of the vortices are driven by parameters, such as the in-plane Alfvèn Mach number that refer to the large-scale plasma structure. In particular the vortices become more rolled up with increasing Mach number, i.e. keeping the velocity field fixed, for weaker in-plane magnetic fields. We show that, varying this parameter, we can control whether the large-scale motion during its evolution is able or not to build up small spatial scales during its evolution. If the in-plane magnetic tension is too high, the large-scale evolution of the vortices is not able to develop such small scales and the system exhibits essentially MHD behavior during all its evolution.

2. Model plasma configuration and governing equations

We start from a two-fluid description of the plasma. Since we assume quasineutrality we can describe the plasma with the following set of two-fluid equations which we write in dimensionless conservative form. The characteristic dimensional quantities are the mass density nm_i, the Alfvén velocity $v_A = (B^2/4\pi n_i m_i)^{1/2}$ and the ion skin depth $d_i \equiv c/\omega_{pi}$, thus $d_e^2 = m_e/m_i$. By summing the electron and proton continuity equations we obtain

$$\partial n/\partial t + \nabla \cdot (n\mathbf{U}) = 0 \tag{1}$$

with $n = n_i = n_e$ the plasma density, $\mathbf{U} = (\mathbf{u_i} + d_e^2 \mathbf{u_e})$ the plasma fluid velocity and $\mathbf{u_{i,e}}$ the ion and electron fluid velocities, respectively. In the low frequency range of interest the displacement current can be disregarded, thus $\mathbf{J} = n\mathbf{u_i} - n\mathbf{u_e} = \nabla \times \mathbf{B}$. By summing the electron and proton equations of motion we obtain:

$$\partial(n\mathbf{U})/\partial t + \nabla \cdot \left[n(\mathbf{u_i u_i} + d_e^2 \mathbf{u_e u_e}) + P_T \bar{\bar{\mathbf{I}}} - \mathbf{BB}) \right] (1 + d_e^2)^{-1} = 0, \tag{2}$$

with $P_T = P_i + P_e + B^2/2$ the total pressure. We consider the isothermal closure

$$\partial P_{i,e}/\partial t + \nabla \cdot (P_{i,e}\mathbf{U}) = 0 \quad \text{thus} \quad P = P_i + P_e = nT_i + nT_e. \tag{3}$$

By properly subtracting the electron and proton equations of motion we obtain a generalized Ohm's law [32]

$$\left(1 + d_e^2 \nabla^2\right) \mathbf{E} = -\mathbf{u_e} \times \mathbf{B} - d_e^2 \left\{ \mathbf{u_i} \times \mathbf{B} + (1/n) \nabla \cdot [n\,(\mathbf{u_i u_i} - \mathbf{u_e u_e})] \right\}, \tag{4}$$

where the term $1/n$ in front of $\nabla^2 \mathbf{E}$ is taken to be constant. Combined with the Faraday equation

$$\partial \mathbf{B}/\partial t = -\nabla \times \mathbf{E},$$

Equation (4) describes the evolution of the magnetic field $\mathbf{B}$. The term $\nabla P_{i,e}/n$ in the generalized Ohm's law has been omitted since, if we assume a polytropic equation of state, it does not contribute to $\nabla \times \mathbf{E}$.

We consider a 2D description of the plasma configuration, with the inhomogeneity direction along x, the homogeneity direction along y and the ignorable direction along z. The sheared velocity field and the in-plane magnetic field are directed along the y-direction, as shown in figure 1. The magnetic field has an out-of-plane component along z. This choice is justified since the evolution of K–H instability in the equatorial plane is only weakly affected

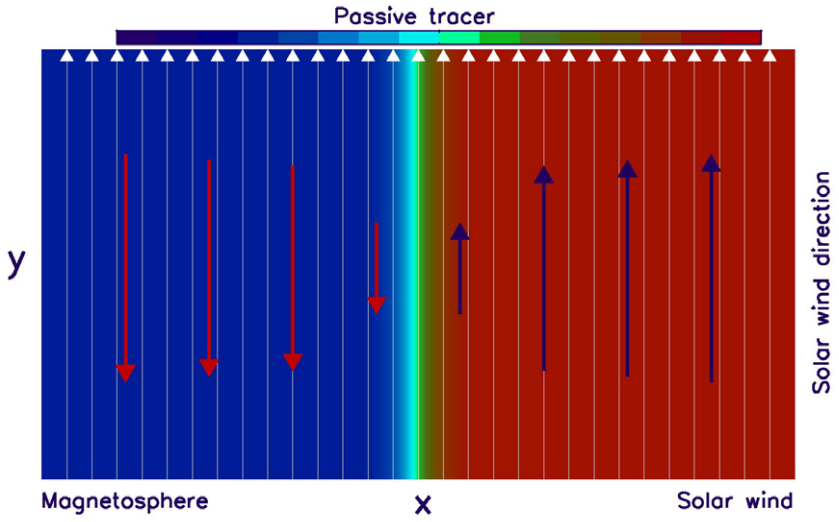

Figure 1. Schematic view of the plasma configuration at $t = 0$. In this homogeneous density configuration the solar wind and the magnetospheric plasmas are represented using red and blue passive tracers with color intensity proportional to the value of the velocity field represented by the black and red arrows. The field lines of the magnetic field in the plane (initially parallel to the flow along the y-axis) are drawn in white. The same color coding is used in subsequent figures.

by a slow equilibrium variation along the z-direction [25]. Since we consider an initial magnetic field with no inversion points, our equilibrium configuration is unstable only against the K–H instability. Other kinds of instabilities (magnetic reconnection and/or the R–T instability) can develop as secondary instabilities only during the nonlinear evolution of the primary K–H. We consider an initial large scale, sheared velocity field given by

$$\mathbf{U}_{\rm eq} = (U_0/2)\ \tanh\left[(x - L_x/2)/L_u\right]\hat{\mathbf{y}}, \tag{5}$$

where L_x is the system dimension along the x-direction and L_u is the half width of the velocity shear. As already stated, since we are primarily interested in VIR, we consider a homogeneous density field in order to eliminate other types of secondary instabilities [29, 30]. The equilibrium magnetic field at $t = 0$ is homogeneous and is taken of the form

$$\mathbf{B}_{\rm eq}(x, y) = B_{\rm eq}\sin\alpha\ \mathbf{e}_y + B_{\rm eq}\cos\alpha\ \mathbf{e}_z, \tag{6}$$

where $B_{\rm eq} = 1.0$. Note that the total pressure $P_{\rm T}$ is spatially uniform at $t = 0$ and that the magnetic field has no inversion points.

The values of the three dimensionless parameters, the sound and Alfvén Mach numbers, are taken as $M_{\rm s} = U_0/C_{\rm s} = 1.0$, $M_{\rm A,\perp} = U_0/U_{\rm A,\perp} = 1/\cos\alpha \simeq 1.0$ and $M_{\rm A,\parallel} = U_0/U_{\rm A,\parallel} = 1/\sin\alpha$, where $5.0 \leqslant M_{\rm A,\parallel} \leqslant 20.0$, with $U_0 = 1.0$, $U_{\rm A,\perp}$ and $U_{\rm A,\parallel}$ the z- and y-components of the equilibrium Alfvén velocity, respectively. The sound and Alfvén Mach numbers $M_{\rm s} = U_0/C_{\rm s}$, $M_{\rm A,\perp} = U_0/U_{\rm A,\perp}$ control the degree of plasma compressibility, while $M_{\rm A,\parallel} = U_0/U_{\rm A,\parallel}$ is a measure of the importance of the magnetic field lines tension in the x, y-plane and thus influences both the linear and nonlinear development of the K–H instability, i.e. how much the

K–H vortices are rolled up. We consider a configuration with a value of the plasma β parameter (defined as the ratio of the plasma pressure over the total magnetic field pressure) of order unity.

3. Numerical procedures, simulation box and boundary conditions

The equations derived in section 2 are integrated by means of a numerical code. This code is based on a standard third-order Adam–Bashforth method for temporal discretization. It uses fast Fourier transform routines [33] for spatial derivative along the periodic y-direction and sixth-order compact finite difference scheme with spectral like resolution for spatial derivative along the inhomogeneous x-direction [34]. Numerical stability is achieved by means of filters, a spectral filter along the periodic y-direction and a sixth-order spectral-like filtering scheme along the inhomogeneous x-direction [34]. These choices, combined with zero resistivity and viscosity in the model equations, allow the large-scale K–H vortices to follow an essentially inviscid evolution and the small-scale magnetic reconnection to be driven essentially by the finite electron mass.

Since we are interested in large-scale K–H vortices, we take $L_u = 3d_\mathrm{i}$. This choice corresponds to a FGM wavelength roughly $5\pi L_u = 15\pi d_\mathrm{i}$ and thus to large scale, nearly MHD vortices [22, 23].

The box length $L_y = 60\pi$ in the periodic y-direction is chosen in order to allow the K–H instability to form five well-developed nonlinear vortices and thus to study the pairing process between these vortices under more general conditions than the ones investigated in [8, 28]. Once the value of L_y has set the size of the final paired vortex, L_x is chosen so as to be compatible with this size. We take $L_x = 120$.

Since we want to resolve the d_e-scale, we take the number of grid points along the x-direction $Nx = 1024$, while along the y-direction $Ny = 1024$. In the simulations, we have adopted a reduced electron–ion mass ratio $m_\mathrm{e}/m_\mathrm{i} = 1/64$.

Special care is devoted to boundary conditions. Although the boundary conditions along the periodic y-direction are straightforward (periodic boundary conditions), along the inhomogeneous x-direction we need transparent boundary conditions in order to let sonic and Alfvénic perturbations, generated by the dynamics induced by the K–H instability, leave the numerical domain. In our system, K–H vortices are essentially large-scale MHD structures [21]–[23], [25] even when the Hall term and electron inertia are included in equation (4). Thus we assume that the system at the x-boundary, far away from the central region, where small-scale dynamics develops, can be described using simplified ideal MHD equations instead of two-fluid equations. Boundary conditions are thus obtained from the ideal MHD set of hyperbolic equations for which it is possible to define the projected characteristics along the x-direction [35]–[37], while it would not be possible instead for the two-fluid set of equations. Once we have defined projected characteristics we know exactly which perturbations are leaving or entering the simulation domain and thus we can build up transparent boundary conditions. A detailed derivation of the boundary condition used are given in appendix A. We stress that the non-reflecting boundary conditions adopted are a key feature of our numerical code. Without these conditions we would not be able to study both the linear and the nonlinear evolution of K–H instability in the presence of an in-plane magnetic field.

4. Simulation results

Since we are interested in the weak field regime, we consider the following three values of the in-plane Alfvén Mach number $M_{A,\parallel} = 20.0$, 10.0 and 5.0. These choices allow the K–H instability to develop into rolled up vortices. As mentioned before, the higher the value of the Alfvèn Mach number, the more rolled up are the vortices.

4.1. Weak magnetic tension regime

This regime, where $M_{A,\parallel} = 20.0$, has been studied in [8, 28] using a simulation box twice as long as the wavelength of the FGM of the K–H instability. This choice permits the development of two highly rolled up vortices and thus is suitable for investigating the competition between the pairing process and the vortex disruption caused by VIR. Here, we recall the main results presented in [8, 28] where the same equilibrium configuration and governing equations given in section 2 were considered.

Firstly, it was shown that under these conditions the VIR process is not capable of disrupting the vortex structures before they coalesce and that magnetic reconnection occurs mainly during the process of vortex pairing. Secondly, it was shown that the motion of the large-scale vortices, which are essentially MHD structures, is capable of creating favorable conditions for reconnection to act and in particular to build up sub-d_i current sheets within which two-fluid effects became effective. In these regions, ions decouple their motion from the evolution of the magnetic field, while electrons decouple from the magnetic field only inside a smaller scale layer determined by electron inertia. Furthermore, the decoupling of the ion and electron dynamics allows the ion inflow velocity, at the reconnection point, to be comparable with the local Alfvén velocity. As a result, fast magnetic reconnection [1]–[7] develops on timescales comparable to the plasma dynamical timescale determined within the ideal MHD description.

This small-scale evolution is not simply superposed to the large-scale evolution but influences and drives the large-scale dynamics. The large-scale motion creates, and can subsequently destroy, the favorable condition for reconnection to occur. If magnetic reconnection develops 'fast' enough, it is able to take advantage of this finite 'time window' and to change the global magnetic topology. When magnetic reconnection starts to act, the evolution of the whole system depends on the specific physical phenomena that occur at small spatial scales and control how 'fast' reconnection develops. In particular fast magnetic reconnection is able to rearrange the global magnetic topology and lets large-scale portions of the plasma enter previously unconnected plasma regions. This interplay between different phenomena provides a clear cut example of the feedback between the large-scale MHD system evolution and the small-scale physics (d_i-scale and d_e-scale). Furthermore, this multiple scale behavior of K–H vortices leads to the formation of *coherent magnetic structures* (magnetic islands) much larger than the electron inertial scale layer but much smaller than the large-scale size of the vortices.

In the present paper, we consider a box setup that allows the K–H instability to develop into more than two rolled up vortices. Thus we can observe several pairing events in the results of the simulations described below. In figures 2 and 3, we show the magnetic field lines projected on the (x, y)-plane and the red–blue colored plasma passive tracer, advected by the fluid velocity field. As previously stated, these large-scale vortices are essentially MHD structures and the magnetic field is essentially advected by the fluid velocity field, except locally in the central region where magnetic reconnection and two-fluid dynamics can occur. This fact

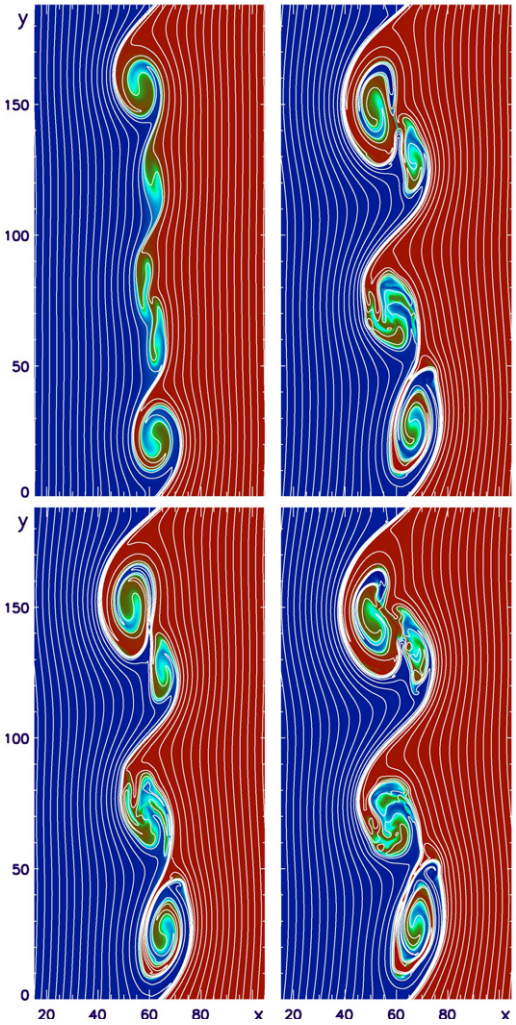

Figure 2. Plasma passive tracer and magnetic field lines in the (x, y)-plane at $t = 335, 380$ (left column, top to bottom), and $t = 395, 410$ (right column, top to bottom), for $M_{\mathrm{A},\parallel} = 20.0$.

is supported by the good correlation between the plasma and the magnetic structures (figure 2). At $t = 335$ we see (figure 2, upper left) the vortices generated by the K–H instability. Although the mode number corresponding to the FGM is $m = 4$, the competition between the $m = 3, 4, 5$ modes generates five unequal vortices. The nearly frozen in magnetic lines are rolled up and compressed by the motion of the vortices. We see the formation of a central 'ribbon' [8] of nearly parallel, compressed magnetic lines, which separates the blue and red plasma regions. The following frames show that the pairing process remains effective. Gradually the five unequal vortices merge and form one big vortex (figure 3, right-bottom), the biggest one allowed within the simulation box. The vortex pairing process is clearly seen also in figure 4, where we plot the time evolution of the amplitude of the first six wave number modes of the plasma velocity field along x.

At $t = 335$, we observe the first pairing process between two adjacent vortices, located at $x = 60$, $y = 70$ (figure 2, upper-left). Although the two pairing vortices are not highly rolled

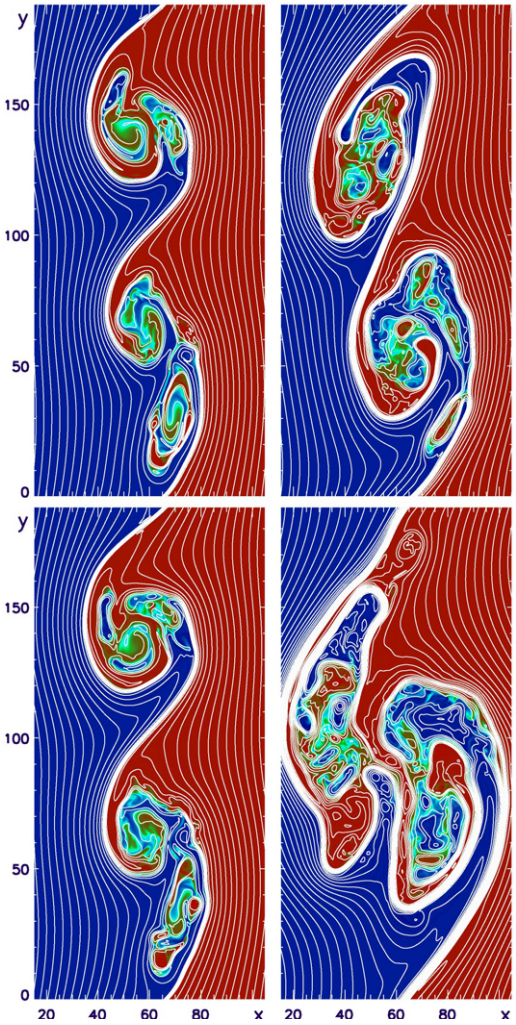

Figure 3. Plasma passive tracer and magnetic field lines in the (x, y)-plane at $t = 430$, 450 (left column), and $t = 550$, 690 (right column), for $M_{A,\parallel} = 20.0$.

up, the pairing process is effective and the magnetic field lines are compressed and folded by the vortex and merging motion. Thus magnetic reconnection can act during this process [8, 28]. In particular reconnection occurs at $x = 62$, $y = 65$, in the region between the two pairing vortices. Since these vortices are not highly rolled up, the magnetic field lines are not strongly compressed, thus sub-d_i current sheets are not formed. In fact we do not observe any fast magnetic reconnection events during the merging. However, magnetic reconnection is able to inject a red plasma *blob* into the blue region. This process is clearly visible at $t = 380$, $x = 65$, $y = 70$ (figure 2, left-bottom), when the two vortices have formed a new, double sized, paired vortex. This is the first reconnection event observed in our simulation. It is important to note that, at this time, magnetic reconnection has not yet occurred inside the two main highly rolled up vortices, located at $x = 60$, $y = 20$ and $x = 60$, $y = 160$. Reconnection will occur there only during subsequent pairing processes, when the favorable conditions for reconnection will be generated not only by the vortex motion but also by the merging process. At $t = 380$, we observe the formation of a X-point at $x = 60$, $y = 142.5$, during the second pairing process between the

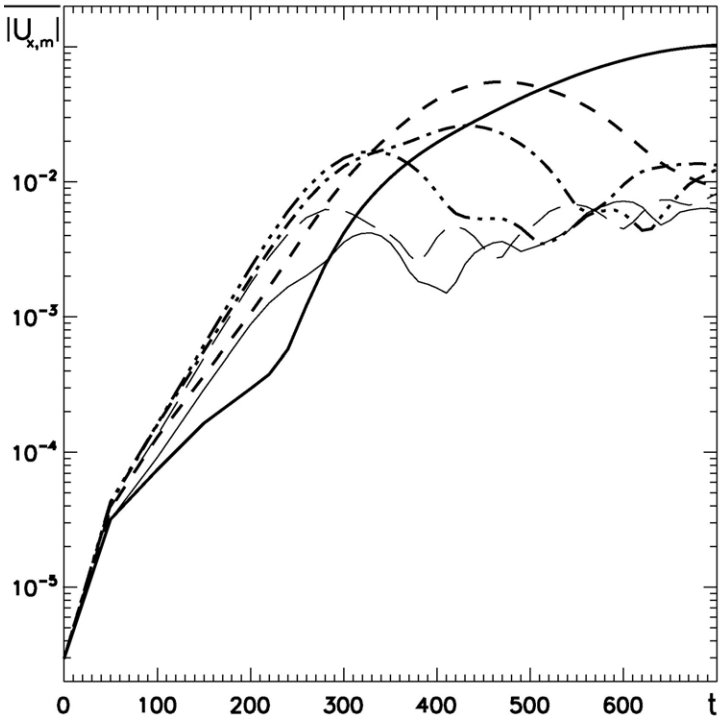

Figure 4. Time evolution of the first six Fourier components of the plasma velocity along x, averaged along x, for $M_{A,\parallel} = 20.0$, $m = 1$ continuous, $m = 2$ dashed, $m = 3$ dash-dotted, $m = 4$ (FGM) dash-three dotted, $m = 5$ thin dashed, $m = 6$ thin continuous. The $m = 1$, 2, 3 and 4 lines have been drawn thicker in order to emphasize the pairing process.

two upper vortices. These merging vortices are highly rolled up, thus the magnetic field lines have been more effectively twisted and compressed by the motion of the vortices and sub-d_i current sheets are formed in the region between the two merging vortices, corresponding to a local magnetic inversion line (figure 5, left-top). It is important to note that magnetic reconnection occurs in the region between the vortices, i.e. where field lines are not only twisted and compressed by the single vortex rolling up, but also by the pairing process. Since the two vortices are unequal, a sub-d_i sheet is formed only on the left side of the central ribbon, thus we observe fast magnetic reconnection only at this position. We observe an inflow plasma velocity at the X-point that is approximately one tenth of the local Alfvén velocity U_a in the (x, y)-plane, as expected in the case of fast magnetic reconnection [2]. We thus infer that the value of the reconnection growth rate is $\gamma \sim 0.1\, U_a/L \sim 0.15$, where L is the shear length of the in-plane magnetic field at the X-point. This inferred value is compatible with the growth rate $\gamma \sim \mathrm{d}\Delta\psi/\mathrm{d}t$ observed in the simulation, where $\Delta\psi$ is the difference between the value of the magnetic flux function at the X-point and at the O-point, located at $x \simeq 60$, $y \simeq 155$.

The absolute maximum value of the current density in this sheet is in normalized units $\sim$1.8 and the width of the sheet is approximately $0.5d_i$. Furthermore, the value of the in-plane magnetic field inside the current sheet is strongly enhanced by the compressional motion of the vortices. In particular, the value of the y-component (essentially the in-plane component, inverted across the current sheet) and the value of the z-component (the guide field in the

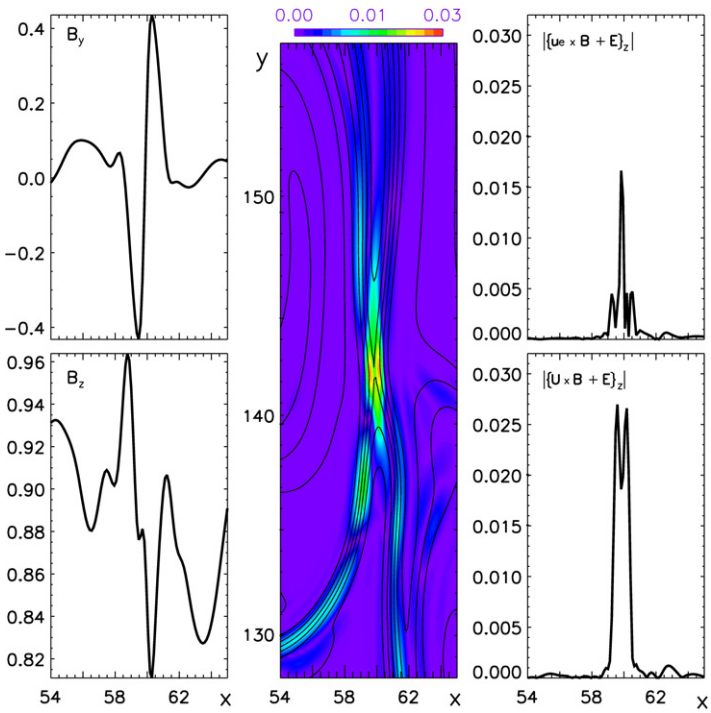

Figure 5. Left frame: the y-component (top) and the z-component (bottom) of the magnetic field, plotted along the x-direction at $y = 142.5$, $t = 385$, for $M_{A,\|} = 20.0$. Central frame: ion decoupling region ($D_i \neq 0$) and magnetic field lines in the region between the two pairing vortices at $t = 385$, $x = 60$, $y = 142$. Right frame: electron (top) and ion (bottom) decoupling region ($D_e \neq 0$ and $D_i \neq 0$, respectively) along the x-direction at $y = 142.5$, $t = 385$.

terminology of magnetic reconnection) are comparable (figure 5, left) while initially the guide to in-plane magnetic field ratio was more than a factor of ten. Thus, in this region, we expect the Hall term to be comparable to the $\mathbf{U} \times \mathbf{B}$ term in Ohm's law. In order to underline its role, we define two quantities, $D_i = |\{\mathbf{U} \times \mathbf{B} + \mathbf{E}\}_z|$ and $D_e = |\{\mathbf{u_e} \times \mathbf{B} + \mathbf{E}\}_z|$, which measure, respectively, the ion and the electron 'decoupling' from the magnetic field. We show a wide ion decoupling region, where $D_i \neq 0$ (figure 5, central). This region extends across the X-point over a few d_i lengths. In the right frames of the same figure, we plot a section at $y = 142.5$ of D_i (bottom) and of D_e (top) at $t = 385$ and show two separate decoupling regions [2], the 'wider' ion decoupling region where $D_i \neq 0$ and $D_e \simeq 0$ and the inner, thinner electron decoupling region where $D_e \neq 0$ of width of the order of a few d_e. Inside the ion decoupling region, of width roughly equal to $1.5d_i$, the magnetic field is essentially frozen in the electron motion but the MHD frozen in law is not satisfied and the two terms $\mathbf{U} \times \mathbf{B}$ and $\mathbf{J} \times \mathbf{B}$ have approximately the same absolute value. Inside the thinner electron region also the electrons are decoupled from the magnetic field and magnetic reconnection can take place.

These two separate regions provide an important signature of fast magnetic reconnection [2]. On the other hand, our results do not provide any clear evidence of the so-called 'Hall quadrupole' [3], [38]–[42] in the spatial structure of B_z near the X-point. This is most likely caused by the large-plasma compression ($\beta \sim 1$) [6] and by the large variation

of B_z [6, 26] which is compressed by the motion of the vortices. This result is important since the 'Hall quadrupole' is often considered as the 'fast reconnection signature' to be retrieved in the satellite data analysis. This signature is visible only in simplified magnetic configurations and in the case of small plasma compression [6]. Magnetic reconnection at the X-point at $x = 60$, $y = 142.5$ acts fast enough [8] to open the central ribbon (figure 2, right-upper). A new ribbon is formed which no longer separates the blue and red plasma regions. In fact we observe an ear-shaped blue blob injected into the red region at $x = 55$, $y = 150$.

At $t = 410$ the two lower vortices start to interact (the vortex located at $x = 55$, $y = 70$ is the product of the first pairing process). This is the third pairing process observed (figure 2, right-bottom). At the same time we observe the formation of a new X-point at $x = 65$, $y = 43$, during this process. Once more, the motion of the two unequal vortices is able to compress the magnetic field lines and form a sub-d_i current sheet, corresponding to a local magnetic inversion line. Also in this case the formation of two different decoupling regions indicates that fast magnetic reconnection acts at this X-point. The intensity and width of this current sheet, the ratio between the inflow velocity and the local Alfvén velocity in the (x, y)-plane, are comparable with those observed at $t = 380$, $x = 60$, $y = 142.5$. As in the case of the second pairing process, fast magnetic reconnection is able to open the ribbon. A new ribbon is thus formed which no longer separates blue and red plasma regions. We observe the injection of a red, ear-shaped blob into the blue region at $x = 65$, $y = 30$ (figure 3 upper-left). During this third pairing process we observe the formation of two X-points inside the current sheet and thus the generation of a magnetic island with a typical size of few d_i [28] at $x = 62$, $y = 30$. This *coherent magnetic structure* is further advected by the fluid velocity but maintains its 'identity' for a long time interval, compared with its formation time.

At $t = 450$ the second and third pairing processes have just been completed. In figure 3 (right-upper), we show two well formed vortices which start to interact and finally merge (figure 3 right-bottom).

4.1.1. Comparison with single vortex simulations. We can compare the previous results with those that we obtain by simulating the evolution of the K–H instability inside a simulation box with $L_y = \lambda_{FGM} = 15\pi$. In this case the FGM corresponds to $m = 1$ and thus the K–H instability forms only one vortex, the largest one contained in the simulations box. The first reconnection events occur at $t = 400$, $x = 23$, $y = 31$ and $x = 34$, $y = 15$ (figure 6, left). At this time the $m = 1$ mode has just begun to decrease its amplitude, due to nonlinear saturation, which is near its local minimum value (figure 6, right). Subsequently the VIR process leads to vortex disruption (figure 6, middle). This evolution is possible only because the vortex is the biggest one allowed by the simulation box size, thus the single vortex cannot follow its 'natural' evolution, i.e. pairing with another vortex. In this case VIR has all the time it needs to disrupt the vortex, and not a 'finite time window'.

If we remove the constraint $L_y = \lambda_{FGM}$ the evolution of the FGM follows an inverse cascade as shown previously. During this process, when an m mode reaches nonlinear saturation, its amplitude is overtaken by the amplitude of the $m - 1$ mode (figure 4). We stress that magnetic reconnection occurs during the saturation of the m mode and its overtaking by the $m - 1$ mode, and not during the evolution of a single vortex. Moreover, reconnection occurs mainly in the region between the two pairing vortices (figures 2 and 3) and not in the inner part of both arms of each vortex (figure 6, left). Thus, reconnection is driven by the motion of the two vortices during the merging process and not by the rolling up of single vortices.

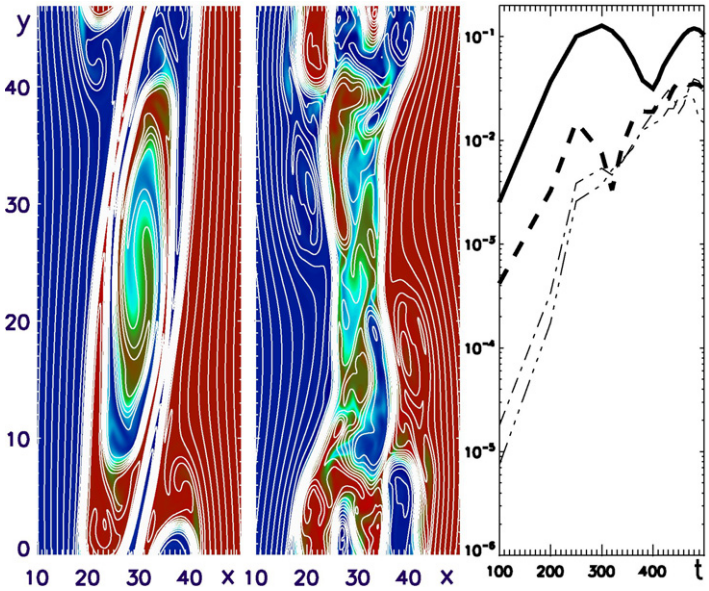

Figure 6. Left and middle frames: plasma passive tracer and magnetic field lines in the (x, y)-plane at $t = 400$ and 450, respectively, for $M_{A,\parallel} = 20.0$ and $L_y = 15\pi$. Right frame: time evolution of the first four Fourier components of the plasma velocity along x, averaged along x, for $M_{A,\parallel} = 20.0$ and $L_y = 15\pi$, $m = 1$ (FGM) continuous, $m = 2$ dashed, $m = 3$ dash-dotted, $m = 4$ dash-three dotted line.

4.1.2. Comparison with MHD results. Here, we discuss the crucial role of the Hall term by running the same multiple vortex simulation parameters simply omitting the Hall term in the generalized Ohm's law (4) ($\mathbf{u_e} \times \mathbf{B} \simeq \mathbf{U} \times \mathbf{B}$). This analysis is similar to the one that was performed in the case of two vortex evolution [8].

Although the large-scale motion of the vortices is still able to generate current sheets of comparable intensity and width, the process of magnetic reconnection occurs on a slower timescale. In particular it does not succeed in cutting the ribbon during the second pairing process. We can see (figure 7, upper-left) that at $t = 400$ the X-point located at $x = 60$, $y = 142.5$ has formed. However, since the reconnection rate is slower, the upper vortices continue to roll up and pair (figure 7, left-bottom, right-upper). The rolling up of the vortices destroys the favorable conditions for the reconnection instability to grow, thus magnetic reconnection is no longer able to cut the ribbon. As a consequence, no plasma injection is observed during the merging. The (ear-shaped) blue blob is no longer topologically connected with the red region (figure 7, right-bottom).

On the contrary, magnetic reconnection at $x = 65$, $y = 43$, occurring during the third pairing process between the two lower vortices (figure 7, left-bottom) is still able to cut the ribbon and to let the red blob enter the blue region (figure 7, right-bottom). Since the Hall term is neglected, this process is slower and the red blob needs about twice the time to enter the blue region, but can still enter. In addition, multiple X-points are not formed during this process, thus magnetic islands of typical size of a few d_i [28] are not generated.

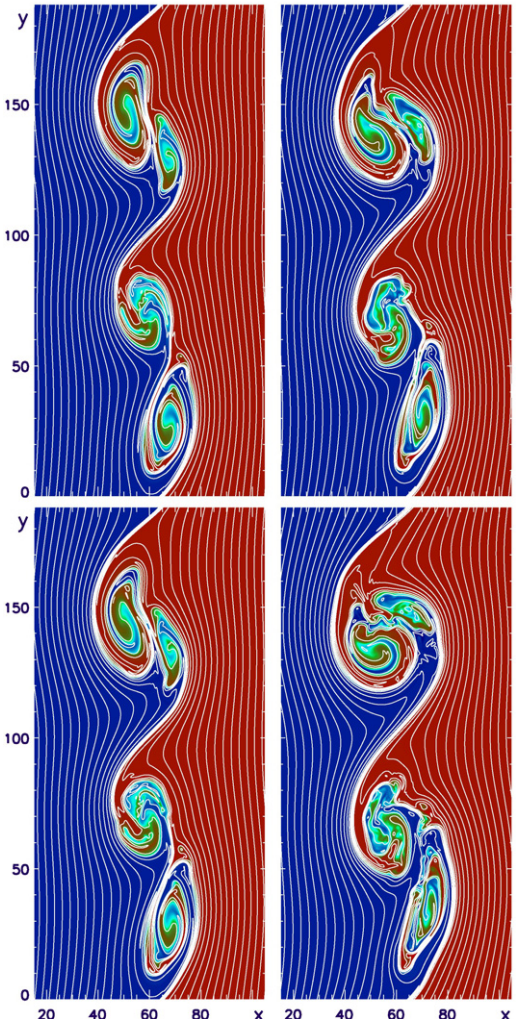

Figure 7. Plasma passive tracer and magnetic field lines in the (x, y)-plane at $t = 400, 410$ (left column), and $t = 430, 450$ (right column), for $M_{\mathrm{A},\parallel} = 20.0$. The Hall term is neglected in the generalized Ohm's law.

This comparison shows that when the rolling up and the pairing of the vortices develop on a timescale comparable with the reconnection time, the competition between the development of the large-scale magnetic configuration and the evolution and the reconnection instability determines the development of the entire system. The early evolution of the vortices is essentially MHD and depends only on the initial velocity and magnetic field, regardless of the specific small-scale physics included in the generalized Ohm's law. On the contrary, as exemplified here by the results obtained by omitting the Hall term, when magnetic reconnection starts to act, the evolution of the whole system depends on the specific physical phenomena (ions and electrons decoupling) that occur at small spatial scales. Large-scale dynamics builds up the favorable conditions for reconnection to occur which in turn influences the evolution of the whole system [8]. This is true during the second pairing process, when the plasma injection is strongly influenced by the small-scale dynamics. On the contrary, the third pairing process is slow enough to let the magnetic reconnection have all the time it needs to act and cut the central

ribbon. This process generates a magnetic topology similar to that obtained in the 'Hall' case. Thus, during the third pairing process, plasma injection is effective also in the slower MHD case. However, coherent structures are not generated when the Hall term is omitted.

4.2. Intermediate magnetic tension regime

We performed a similar simulation choosing $M_{A,\parallel} = 10.0$. The corresponding value of the magnetic tension allows the K–H instability to develop in fully rolled up vortices, as for the case discussed in the previous section.

These vortices exhibit similar phenomena and trends and in particular multiple scale behavior and strong feedback between the large- and small-scale dynamics. The vortex motion creates, during subsequent pairing processes, the necessary conditions for magnetic reconnection to occur and for two-fluid dynamics to develop. In particular the folding of the central ribbon and the plasma compression allow fast magnetic reconnection to cut the magnetic field line ribbon 'fast' enough and to connect the two regions of initially magnetically unconnected plasma.

4.3. Near threshold regime

Here we take $M_{A,\parallel} = 5.0$. This value is close to the threshold at which the generation of rolled up vortices by the K–H instability is suppressed. For lower values of $M_{A,\parallel}$ magnetic tension is strong enough to provide nonlinear stability [18]–[21] preventing the formation of rolled up vortices. Nevertheless, for $M_{A,\parallel} = 5.0$, the vortices are still able to roll up the magnetic field lines and to build up magnetic inversion layers. On the contrary the vortex motion is no longer capable of folding the central ribbon.

At $t = 305$, we show (figure 8, upper-left) wave-like perturbations of the fields. At $t = 370$ (figure 8, left-bottom), during the nonlinear evolution, two of these perturbations develop into rolled up vortices, while the others maintain their wave-like behavior. The wave-like perturbation located at $x = 60$, $y = 125$ is simply absorbed, engulfed, without reconnection, by the upper vortex. The perturbation located at $x = 60$, $y = 80$ is generated by the merging of two 'shorter' wave-like perturbations and eventually develops into a rolled up vortex which starts to interact and pair with the lower one (figure 8, right-upper). Due to the higher value of magnetic tension the ribbon is not folded by the motion of the vortices and it does not exhibit any inversion layer. Therefore magnetic reconnection cannot develop in this region and thus cannot cut the ribbon and connect the two regions. Magnetic reconnection occurs only on the right and on the left of the central ribbon (figure 8, right-bottom) and red–blue plasma blobs do not enter the blue–red region. Furthermore, the magnetic field lines are not highly rolled up and compressed and sub-d_i current sheets are not formed. Consequently we do not observe fast magnetic reconnection and in particular we do not observe two separated magnetic decoupling regions for ions and electrons.

At $t = 500$ this pairing process has been completed (figure 9, upper-left). Then, the wave-like perturbation formed, located at $x = 60$, $y = 80$, develops into a rolled up vortex and starts to interact with the upper vortex (figure 9, left-bottom). As was the case during the previous pairing process, magnetic tension prevents the formation of sub-d_i current sheets and does not allow the plasma motion to fold the central ribbon. Thus magnetic reconnection does not cut the ribbon and we do not observe any plasma injection (figure 9, right-upper). Finally the two vortices merge together (figure 9, right-bottom).

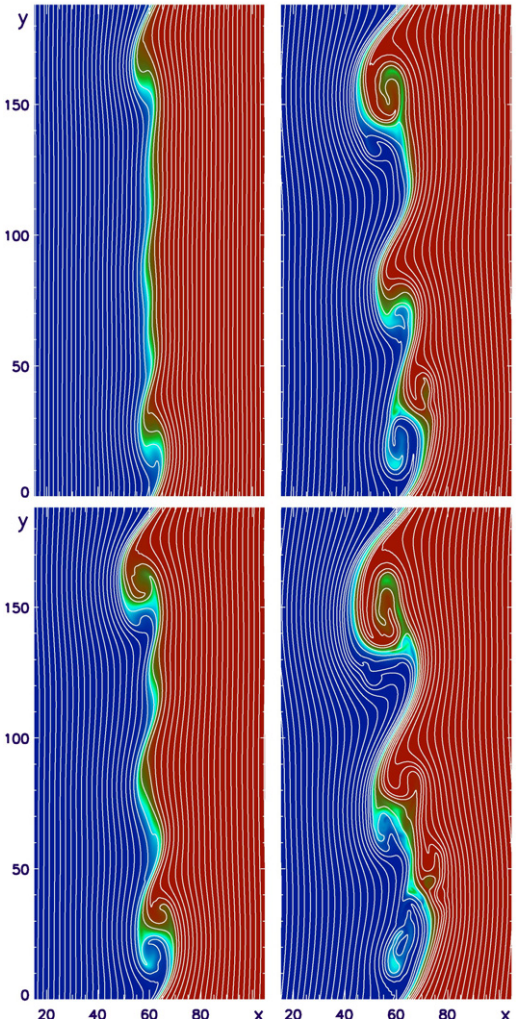

Figure 8. Plasma passive tracer and magnetic field lines in the (x, y)-plane at $t = 305, 370$ (left column), and $t = 430, 480$ (right column), for $M_{A,\parallel} = 5.0$.

Here we remark that, in this near to threshold regime, the specific physical phenomena that occur at small spatial scales do not influence the plasma injection, i.e. the large-scale evolution. The higher value of magnetic tension prevents the folding of the central ribbon, which is a necessary condition for plasma injection. Reconnection occurs only around the vortex arms, on the left and on the right of the central ribbon, i.e. inside each region of unconnected plasma. For this reason in this regime how fast reconnection acts is not crucial.

Furthermore, the magnetic tension prevents the plasma compression and thus the formation of sub-d_i current sheets during large-scale motion. Thus fast magnetic reconnection cannot develop and the vortices maintain their MHD behavior throughout. In this regime the large-scale motion does not create the favorable condition for plasma injection and for the development of two-fluid dynamics.

It is important to note that the pairing process is still effective (figure 10) and, as in the previous cases, VIR is not able to destroy the vortices before they coalesce. Magnetic reconnection occurs mainly during pairing processes between adjacent vortices, instead of inside a single rolled up vortex.

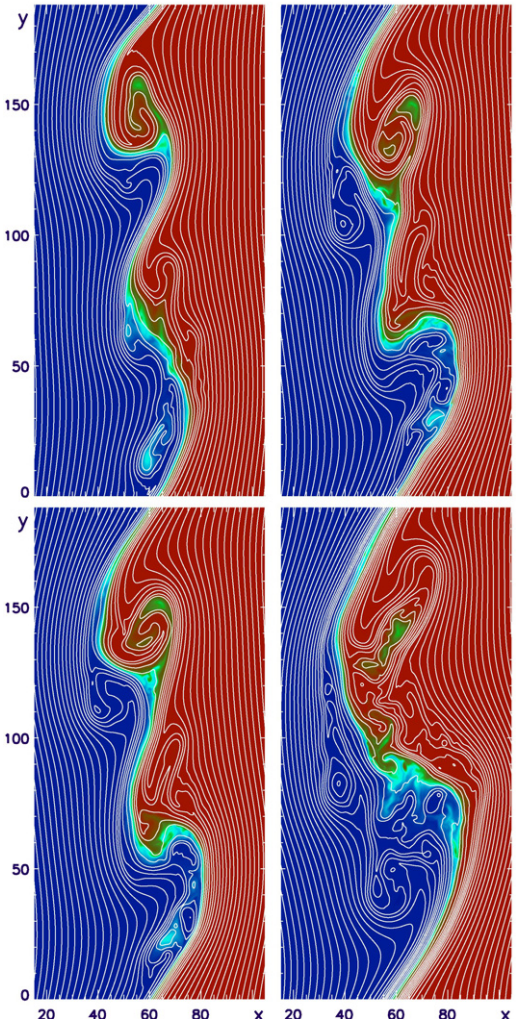

Figure 9. Plasma passive tracer and magnetic field lines in the (x, y)-plane at $t = 500, 570$ (left column), and $t = 600, 700$ (right column), for $M_{A,\parallel} = 5.0$.

4.3.1. Comparison with single vortex simulations and with MHD simulations. Comparing the results obtained above with the evolution of a single vortex in the near to threshold regime leads to the same conclusions discussed in sections 4.1.

Since the large-scale motion is not able to build up sub-d_i current sheets, in this regime the Hall term in the generalized Ohm's law (2) does not play any role. The magnetic field is essentially frozen in the ion motion. Thus there is no difference between simulations with or without the Hall term in the generalized Ohm's law.

5. Conclusions

Two dimension two-fluid simulations have been performed in order to investigate further the competition between vortex pairing [12]–[17] and vortex disruption caused by VIR [18]–[23], [26, 27] and thus to understand the nonlinear evolution of the K–H instability better. The model presented is suitable for investigating the generation of a mixing layer at the flank magnetosphere at low latitude during northward periods [9]–[12].

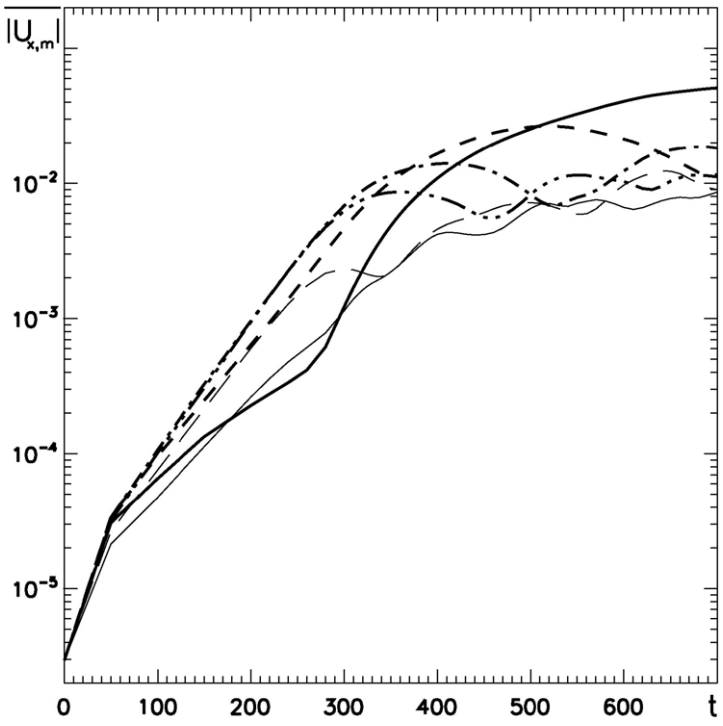

Figure 10. Time evolution of the first six Fourier components of the plasma velocity along x, averaged along x, for $M_{A,\parallel} = 5.0$, $m = 1$ continuous, $m = 2$ dashed, $m = 3$ dash-dotted, $m = 4$ (FGM) dash-three dotted, $m = 5$ thin dashed, $m = 6$ thin continuous. The $m = 1$, 2, 3 and 4 lines have been drawn thicker in order to emphasize the pairing process.

In order to explore the whole 'disruptive' regime [18]–[21] the value of the in-plane Alfvénic Mach number $M_{A,\parallel}$ has been varied from 20.0 to 5.0, within which range the K–H instability develops into rolled up vortices. This number refers to our simplified model which assumes a uniform initial density and magnetic field. This choice excludes other types of secondary HD instabilities [29, 30], which can compete effectively with the pairing process and can disrupt the vortices before they merge [30]. Our model is chosen so as to underline the competition between VIR and the pairing process. Magnetic reconnection is actually driven by the motion of the vortices, since the initial magnetic field does not exhibit any inversion line, which are built only by the evolution of the primary K–H instability.

Compared with previous studies [8, 28] that focused on the competition between pairing process and VIR, in the present paper we consider a bigger simulation domain along the periodicity direction. This choice allows the K–H instability, entering the nonlinear stage, to develop more than two vortices. This allows us to study this competition during four subsequent pairing processes between unequal vortices, a configuration that describes the evolution of the real system better. Although the evolution of this wider configuration is rather less symmetric compared with the evolution of the two equal vortices [8, 28], similar phenomena and trends are recovered.

Contrary to previous single vortex studies [18]–[20], [22, 23, 26, 27], we show that in the 'disruptive' regime, not only is VIR not capable of disrupting vortices before they coalesce, but also that magnetic reconnection occurs mainly during the pairing process. Magnetic

reconnection is driven by the pairing process instead of being driven by the motion of each single vortex.

The key point is how fast reconnection develops, compared with the large-scale characteristic timescale. The competition between the global system and the reconnection timescale influences the large-scale magnetic topology, and thus the final configuration. Magnetic reconnection has a finite 'time window' to cut the central magnetic ribbon, which separates two initially magnetically unconnected regions, before the large-scale motion destroys the favorable conditions that it has just created. This 'time window' is crucial for the feedback between the large-scale motion and the small-scale dynamics to take place. On the other hand, in the framework of single vortex simulations it is not possible to investigate the interaction between large- and small-scale dynamics. In this case, indeed, the vortex, the biggest one allowed by the simulation box size, cannot pair with other vortices and, once it has reached nonlinear saturation, simply becomes an 'imposed' structure that reconnection can only destroy, leading to the formation of a mixing layer. Obviously this evolution is quite 'unrealistic', since a possible and effective evolution of the system (vortex pairing) is not allowed to occur because of a numerical artifact. In the multiple vortex case VIR cannot generate by itself a true mixing layer between the magnetospheric and the solar wind plasma, which is likely generated by subsequent pairing processes (that also drive magnetic reconnection), or by the onset of effectively secondary hydrodynamic instabilities [29, 30].

Magnetic reconnection, which obviously occurs only locally, is able to influence the evolution of the whole system. In particular magnetic reconnection is able to change the global magnetic field topology and thus to 'connect' different regions which were 'unconnected' (i.e. magnetosphere and solar wind region) [8]. The favorable conditions for the reconnection instability to grow are provided by the large-scale motion, i.e. the vortices rolling up and pairing. The necessary condition for connecting these two regions is that the central ribbon, a region of nearly parallel, compressed magnetic lines that separates these regions, is folded by the motion of the vortices. In this case magnetic reconnection can act inside the current sheets formed by the folded ribbon, cut the ribbon and connect these two regions. This process occurs during the merging between two adjacent vortices and lets a significant portion (blob) of plasma enter the 'opposite' region. This necessary condition is built up by the motion of the vortices only when the in-plane magnetic tension is low enough. In fact the central ribbon is cut and the two regions are connected when $M_{A,\parallel} = 20.0, 10.0$. When $M_{A,\parallel} = 5.0$ the magnetic tension is too large, the motion of the vortices is not able to fold the central ribbon and create an inversion layer for the magnetic field. Thus magnetic reconnection cannot cut the ribbon. In this case magnetic reconnection occurs only inside each region, inside the vortex arms and cannot connect these two region. Thus full rolled up vortices are necessary seeds for plasma mixing.

Although large-scale physics builds up the conditions for reconnection to occur, the specific physical phenomena that occur at small spatial scales, and drive magnetic reconnection, can influence the final magnetic topology, see appendix B, where a comparison with the resistive case is also made. When the pairing vortices are able to create sub-d_i current sheets, ions can decouple their motion from the evolution of the magnetic field. This is caused by the two-fluid nature of our plasma model, and is not possible in a simpler MHD description of the plasma. Thus higher ion inflow velocity, and reconnection rates, are possible. For this reason this process is know as fast magnetic reconnection [2]–[6], [8, 28]. In particular fast magnetic reconnection sets up spontaneously during the pairing process, without any need of special boundary conditions or initial conditions.

Since magnetic reconnection develops on a timescale comparable with that of the pairing process, how fast the reconnection occurs becomes crucial. If magnetic reconnection is fast enough, the central ribbon can be cut and the magnetosphere and the solar wind region connected [8]. If it is not fast enough, the evolution of the vortices can destroy the favorable condition for reconnection instability to grow, which thus can no longer cut the ribbon and let plasma blobs enter the 'opposite' region. This provides a clear cut example of feedback between large-scale and small-scale physics and underlines the necessity of adopting a multiple scale analysis for such large-scale structures.

While the folding of the central ribbon is a necessary condition for plasma injection, the two-fluid behavior at small spatial scales is not. Nevertheless, when we observed fast magnetic reconnection events (see sections 4.1 and 4.2), these processes not only allow the plasma injection to be faster, compared to MHD simulations, but also, in some regimes, were crucial for plasma injection, which was not observed in the corresponding MHD simulations.

During the pairing process, fast magnetic reconnection is able to generate coherent magnetic structures (magnetic islands). The islands have a typical width $\sim d_{\mathrm{i}}$, which is comparable to the length scale of the magnetic shear layer formed between the two pairing vortices, much larger than the inertial electron length scale d_{e} and much smaller than the full system size. These *coherent magnetic structures* are further advected by the fluid velocity but maintain their 'identity' for a long-time interval, compared with their formation time.

The plasma injection is a change in the global magnetic field topology related to the plasma motion and is actually observed in the low latitude magnetopause. In fact an increase of the solar wind plasma content in the outer magnetosphere during northward magnetic field periods is observed [10, 43, 44].

Acknowledgments

This work was supported in part by PRIN 2006 and by ASI contract I/016/07/0. We are pleased to acknowledge the CINECA super computing center (Bologna, Italy), where part of the simulations was performed. We wish to thank Simone Landi for his helpful suggestion during the development of the non-reflective boundary conditions. Thanks are also due to Carlo Cavazzoni for his help in improving the numerical code.

Appendix A. Boundary conditions

In our dimensionless variable, the MHD equations are: $\partial n/\partial t + \nabla \cdot (n\mathbf{U}) = 0$, $\partial \mathbf{U}/\partial t + \mathbf{U} \cdot \nabla \mathbf{U} = -\nabla P + (\nabla \times \mathbf{B}) \times \mathbf{B}$, $\partial \mathbf{B}/\partial t = \nabla \times (\mathbf{U} \times \mathbf{B})$, with $P = P_{\mathrm{i}} + P_{\mathrm{e}} = nT_{\mathrm{e}} + nT_{\mathrm{i}}$. Since the ideal MHD equations are a set of hyperbolic partial differential equations [35], we can define the projected characteristic along the x-direction as

$$\mathcal{L}_f^+ = (U_x + f)\left\{\alpha_1\left(\frac{1}{f}\frac{T}{n}\frac{\partial n}{\partial x} + \frac{\partial U_x}{\partial x}\right) + \alpha_2\left[\frac{1}{\sqrt{n}}\left(\frac{a_z}{a_\perp}\frac{\partial B_z}{\partial x} + \frac{a_y}{a_\perp}\frac{\partial B_y}{\partial x}\right)\right.\right.$$
$$\left.\left. - \frac{a_x}{f}\left(\frac{a_z}{a_\perp}\frac{\partial U_z}{\partial x} + \frac{a_y}{a_\perp}\frac{\partial U_y}{\partial x}\right)\right]\right\},$$

$$\mathcal{L}_a^+ = (U_x + \xi a_x)\left[\frac{a_y}{a_\perp}\frac{\partial U_z}{\partial x} - \frac{a_z}{a_\perp}\frac{\partial U_y}{\partial x} - \frac{\xi}{\sqrt{n}}\left(\frac{a_y}{a_\perp}\frac{\partial B_z}{\partial x} - \frac{a_z}{a_\perp}\frac{\partial B_y}{\partial x}\right)\right],$$

$$\mathcal{L}_s^+ = (U_x + s)\left\{-\alpha_2\left[\frac{1}{c_s}\left(\frac{T}{n}\frac{\partial n}{\partial x}\right) + \xi\frac{a_x}{f}\frac{\partial U_x}{\partial x}\right] + \alpha_1\left[\frac{c_s}{f\sqrt{n}}\left(\frac{a_z}{a_\perp}\frac{\partial B_z}{\partial x} + \frac{a_y}{a_\perp}\frac{\partial B_y}{\partial x}\right)\right.\right.$$
$$\left.\left. -\xi\left(\frac{a_z}{a_\perp}\frac{\partial U_z}{\partial x} + \frac{a_y}{a_\perp}\frac{\partial U_y}{\partial x}\right)\right]\right\},$$

$$\mathcal{L}_s^- = (U_x - s)\left\{-\alpha_2\left[\frac{1}{c_s}\left(\frac{T}{n}\frac{\partial n}{\partial x}\right) - \xi\frac{a_x}{f}\frac{\partial U_x}{\partial x}\right] + \alpha_1\left[\frac{c_s}{f\sqrt{n}}\left(\frac{a_z}{a_\perp}\frac{\partial B_z}{\partial x} + \frac{a_y}{a_\perp}\frac{\partial B_y}{\partial x}\right)\right.\right.$$
$$\left.\left. +\xi\left(\frac{a_z}{a_\perp}\frac{\partial U_z}{\partial x} + \frac{a_y}{a_\perp}\frac{\partial U_y}{\partial x}\right)\right]\right\},$$

$$\mathcal{L}_a^- = (U_x - \xi a_x)\left[\frac{a_y}{a_\perp}\frac{\partial U_z}{\partial x} - \frac{a_z}{a_\perp}\frac{\partial U_y}{\partial x} + \frac{\xi}{\sqrt{n}}\left(\frac{a_y}{a_\perp}\frac{\partial B_z}{\partial x} - \frac{a_z}{a_\perp}\frac{\partial B_y}{\partial x}\right)\right],$$

$$\mathcal{L}_f^- = (U_x - f)\left\{\alpha_1\left(\frac{1}{f}\frac{T}{n}\frac{\partial n}{\partial x} - \frac{\partial U_x}{\partial x}\right) + \alpha_2\left[\frac{1}{\sqrt{n}}\left(\frac{a_z}{a_\perp}\frac{\partial B_z}{\partial x} + \frac{a_y}{a_\perp}\frac{\partial B_y}{\partial x}\right)\right.\right.$$
$$\left.\left. +\frac{a_x}{f}\left(\frac{a_z}{a_\perp}\frac{\partial U_z}{\partial x} + \frac{a_y}{a_\perp}\frac{\partial U_y}{\partial x}\right)\right]\right\}.$$

Here we have taken $\partial/\partial z = 0$, $a_{x,y,z}$ are the three components of the Alfvén velocity, a its absolute value, $a_\perp^2 = a_y^2 + a_z^2$, $\xi = a_x/|a_x|$, f and s the fast and slow magnetoacoustic velocities, $c_s^2 = T = T_\mathrm{i} + T_\mathrm{e}$, $\alpha_1 = [(f^2 - a_x^2)/(f^2 - s^2)]^{1/2}$ and $\alpha_2 = [(f^2 - c_s^2)/(f^2 - s^2)]^{1/2}$. Thus the above MHD equations can be rewritten as

$$\frac{\partial n}{\partial t} = n\left[\frac{\alpha_2}{2c_s}\left(\mathcal{L}_s^+ + \mathcal{L}_s^-\right) - \frac{\alpha_1}{2f}\left(\mathcal{L}_f^+ + \mathcal{L}_f^-\right)\right] - \frac{\partial}{\partial y}(nU_y),$$

$$\frac{\partial U_x}{\partial t} = \frac{s\alpha_2}{2c_s}\left(\mathcal{L}_s^+ - \mathcal{L}_s^-\right) - \frac{\alpha_1}{2}\left(\mathcal{L}_f^+ - \mathcal{L}_f^-\right) - U_y\frac{\partial U_x}{\partial y} + B_y\frac{\partial B_x}{\partial y}.$$

$$\frac{\partial U_y}{\partial t} = \frac{a_z}{2a_\perp}\left(\mathcal{L}_a^+ + \mathcal{L}_a^-\right) + \frac{a_y}{a_\perp}\left[\frac{\xi\alpha_1}{2}\left(\mathcal{L}_s^+ - \mathcal{L}_s^-\right) + \frac{a_x\alpha_2}{2f}\left(\mathcal{L}_f^+ - \mathcal{L}_f^-\right)\right] - \frac{\partial P}{\partial y} - B_x\frac{\partial B_x}{\partial y} - B_z\frac{\partial B_z}{\partial y},$$

$$\frac{\partial U_z}{\partial t} = -\frac{a_y}{2a_\perp}\left(\mathcal{L}_a^+ + \mathcal{L}_a^-\right) + \frac{a_z}{a_\perp}\left[\frac{\xi\alpha_1}{2}\left(\mathcal{L}_s^+ - \mathcal{L}_s^-\right) + \frac{a_x\alpha_2}{2f}\left(\mathcal{L}_f^+ - \mathcal{L}_f^-\right)\right] + B_y\frac{\partial B_z}{\partial y},$$

$$\frac{\partial B_y}{\partial t} = -\xi\frac{\sqrt{n}a_z}{2a_\perp}\left(\mathcal{L}_a^+ - \mathcal{L}_a^-\right) - \frac{\sqrt{n}a_y}{a_\perp}\left[\frac{c\alpha_1}{2f}\left(\mathcal{L}_s^+ + \mathcal{L}_s^-\right) + \frac{\alpha_2}{2}\left(\mathcal{L}_f^+ + \mathcal{L}_f^-\right)\right] - U_y\frac{\partial B_y}{\partial y},$$

$$\frac{\partial B_z}{\partial t} = \xi \frac{\sqrt{n} a_y}{2 a_\perp} \left(\mathcal{L}_a^+ - \mathcal{L}_a^-\right) - \frac{\sqrt{n} a_z}{a_\perp} \left[\frac{c\alpha_1}{2f}\left(\mathcal{L}_s^+ + \mathcal{L}_s^-\right) + \frac{\alpha_2}{2}\left(\mathcal{L}_f^+ + \mathcal{L}_f^-\right)\right] + B_y \frac{\partial U_z}{\partial y} - B_z \frac{\partial U_y}{\partial y} - U_y \frac{\partial B_z}{\partial y}.$$

The equation for B_x, i.e. the x-component of the Faraday equation, remains unchanged since it does not contain the operator $\partial/\partial x$. In our code all MHD variables (n, $\mathbf{U}$, $\mathbf{B}$) at the x-boundary are advanced using these ideal MHD equations. The other physical variables ($P_{\mathrm{i,e}}$, $\mathbf{J}$, $\mathbf{u_{i,e}}$), as before, are simply deduced using equation (3) and the definitions of $\mathbf{U}$ and of $\mathbf{J}$ in section 2.

In order to solve equation (4), we impose at the boundary $\mathbf{E} = -\mathbf{u_e} \times \mathbf{B} - d_e^2\{\mathbf{u_i} \times \mathbf{B} + (1/n)\nabla \cdot [n(\mathbf{u_i u_i} - \mathbf{u_e u_e})]\}$, where we retain small two-fluid corrections in order to match more accurately the value of the electric field at the boundary, calculated using the simplified MHD description, and its value in the inner part of the simulation box, calculated using the two-fluid model.

These choices allow us to build transparent boundary condition in the inhomogeneity x-direction: in the above equations $\partial/\partial x$ is calculated using only internal points, while Hedstrom's non-reflecting boundary conditions are imposed [35]–[37]: $\mathcal{L}_f^+ = 0$ if $u_x + f < 0$, $\mathcal{L}_a^+ = 0$ if $u_x + \xi a_x < 0$, $\mathcal{L}_s^+ = 0$ if $u_x + s < 0$, $\mathcal{L}_s^- = 0$ if $u_x - s < 0$, $\mathcal{L}_a^- = 0$ if $u_x - \xi a_x < 0$, $\mathcal{L}_f^- = 0$ if $u_x - f < 0$ at the left boundary, and, correspondingly > 0 at the right boundary. In this way any large-scale perturbation that reaches the x-boundary from inside the simulation box can leave it without being reflected.

We stress that simpler numerical boundary conditions, which impose $\partial/\partial x = 0$, or $\partial^2/\partial x^2 = 0$ at the boundary, or which simply calculate $\partial/\partial x$ using only the internal points without using the procedure described before, are partially reflective. Without the adoption of non-reflecting boundary conditions we would be forced to stop our simulations even before the end of the linear phase of the plasma evolution.

The validity of the non-reflecting boundary conditions was tested by studying the injection and propagation of MHD travelling waves (shear Alfvén, fast and slow magnetosonic) with different frequencies and with different equilibrium magnetic configurations. An even more important proof or their validity is given by the fact that we do not observe any change in the numerical results we obtain on the nonlinear system dynamics when we vary the box length L_x in the inhomogeneous direction, provided $L_x \geqslant L_\mathrm{f}$, where L_f is the size of the final paired vortex in the x-direction.

Appendix B. Influence of 'microscopic physics'

How 'fast' reconnection occurs at the inversion layers influences the final evolution of the whole system. The specific phenomena that allow electron decoupling at the scale at which reconnection occurs can influence the rate of the reconnection. For this reason we consider different values of the reduced mass ratio $m_\mathrm{i}/m_\mathrm{e} = d_\mathrm{e}^{-2}$ and compare the collisionless results which those obtained considering a resistive plasma model. In the resistive model the collisionless Ohm's law, equation (4), is replaced by a resistive Ohm's law (without electron inertia) either with the Hall term included (two-fluid description) $\mathbf{E} + \mathbf{U} \times \mathbf{B} - \mathbf{J} \times \mathbf{B} = \eta \mathbf{J}$, or without the Hall term (single fluid description, resistive MHD) $\mathbf{E} + \mathbf{U} \times \mathbf{B} = \eta \mathbf{J}$. We consider values of the normalized resistivity that are compatible with the estimate $\eta \simeq \gamma\, d_\mathrm{e}^2$.

All these results are obtained in the case of two vortices, similarly to [8] and are summarized in the following table:

Reduced mass ratio	25	64	100
One-fluid	'Slow'	'Slow'	'Slow'
Two-fluid	'Fast'	'Fast'	'Fast'
Resistivity	0.01	0.002	0.001
Single-fluid	Diffusive	'Slow'	'Slow'
Two-fluid	Diffusive	'Fast'	'Slow'

We see that, although these results are not asymptotic, the value of the reduced mass ratio does not influence the rate of the reconnection significantly (comparable to the large-scale motion). On the contrary the single- or two-fluid behavior of the plasma, allowing 'ordinary' reconnection or fast magnetic reconnection, is crucial.

In the resistive model, the Hall term continues to influence the reconnection rate significantly, but the specific value of the normalized resistivity is important. If this value is too high ($\eta \sim 0.01$) magnetic diffusion effects become too important. We can no longer distinguish global MHD behavior and a local magnetic reconnection since the magnetic field lines are not well frozen in the fluid motion. For intermediate value of the normalized resistivity ($\eta \sim 0.002$) we obtain results similar to the collisionless model. The Hall term allows reconnection to occur on a timescale that is comparable to that set by large-scale motion. On the contrary, if the value of resistivity is smaller ($\eta \sim 0.001$) the reconnection is too 'slow' even if the Hall term is included in the generalized Ohm's law and cannot change the global topology.

References

[1] Mandt M E *et al* 1994 *Geophys. Res. Lett.* **21** 73
[2] Shay M A *et al* 1998 *J. Geophys. Res.* **103** 9165
[3] Uzdensky D A *et al* 2006 *Phys. Plasmas* **13** 062305
[4] Vekstein G *et al* 2006 *Phys. Plasmas* **13** 122105
[5] Bian N *et al* 2007 *Phys. Plasmas* **14** 072107
[6] Bian N *et al* 2007 *Phys. Plasmas* **14** 120702
[7] Attico N *et al* 2000 *Phys. Plasmas* **7** 2381
[8] Faganello M *et al* 2008 *Phys. Rev. Lett.* **101** 175003
[9] Miura A 1982 *Phys. Rev. Lett.* **16** 779
[10] Hasegawa H *et al* 2004 *Nature* **430** 755
[11] Fairfield D H *et al* 2000 *J. Geophys. Res.* **105** 21159
[12] Otto A *et al* 2000 *J. Geophys. Res.* **105** 21175
[13] Winant C D *et al* 1974 *J. Fluid Mech.* **63** 237
[14] Browand F K *et al* 1976 *J. Fluid Mech.* **76** 127
[15] Miura A 1997 *Phys. Plasmas* **4** 2871
[16] Miura A 1999 *J. Geophys. Res.* **104** 395
[17] Miura A 1999 *Geophys. Res. Lett.* **26** 409
[18] Malagoli A *et al* 1996 *Astrophys. J.* **456** 708
[19] Frank A *et al* 1996 *Astrophys. J.* **460** 777
[20] Jones T W *et al* 1997 *Astrophys. J.* **482** 230
[21] Baty H *et al* 2003 *Phys. Plasmas* **10** 4661

[22] Nakamura T K M *et al* 2005 *Geophys. Res. Lett.* **32** L21102
[23] Nakamura T K M *et al* 2006 *Adv. Space. Res.* **37** 522
[24] Chacon L *et al* 2003 *Phys. Lett.* A **308** 187
[25] Hashimoto C *et al* 2006 *Adv. Space. Res.* **37** 527
[26] Nykyri K *et al* 2004 *Ann. Geophys.* **22** 935
[27] Min K W *et al* 1996 *Geophys. Res. Lett.* **23** 3667
[28] Faganello M *et al* 2008 *Phys. Rev. Lett.* **101** 105001
[29] Matsumoto Y *et al* 2004 *Geophys. Res. Lett.* **31** L02807
[30] Faganello M *et al* 2008 *Phys. Rev. Lett.* **100** 015001
[31] Nakamura T K M *et al* 2008 *Phys. Rev. Lett.* **101** 165002
[32] Valentini F *et al* 2007 *J. Comput. Phys.* **225** 753
[33] Canuto C *et al* 1988 *Spectral Methods in Fluid Dynamics (Springer Series In Computational Physics)* (New York: Springer)
[34] Lele S K 1992 *J. Comput. Phys.* **103** 16
[35] Thompson K W 1987 *J. Comput. Phys.* **68** 1
[36] Hedstrom G W 1979 *J. Comput. Phys.* **30** 222
[37] Landi S *et al* 2005 *Astrophys. J.* **624** 392
[38] Oieroset M *et al* 2001 *Nature* **412** 414
[39] Nagai T *et al* 2001 *J. Geophys. Res.* **106** 25929
[40] Mozer F S *et al* 2002 *Phys. Rev. Lett.* **89** 015002
[41] Vaivads A *et al* 2004 *Phys. Rev. Lett.* **93** 105001
[42] Retinó A *et al* 2007 *Nat. Phys.* **3** 236
[43] Mitchell D G 1987 *J. Geophys. Res.* **92** 7394
[44] Hasegawa H *et al* 2004 *Geophys. Res. Lett.* **431** L06802